Journal of Computational Applied Mechanics 2021, 52(4): 642-663
DOI: 10.22059/jcamech.2021.333435.661

RESEARCH PAPER

Nonlinear coupled torsional-radial vibration of single-walled carbon nanotubes using numerical methods

Zahra Azimzadeh[1], Alireza Fatahi-Vajari[2], Mohammad Reza Ebrahimian[3,*] and Mojtaba Shariati[4]

[1] *Department of Mathematics, Yadegar-e-Imam Khomeini (RAH) Shahre Rey Branch, Islamic Azad University, Tehran, Iran*
[2] *Department of Mechanical Engineering, Shahryar Branch, Islamic Azad University, Shahryar, Iran*
[3] *Department of Mechanical Engineering, Kar Higher Education Institute, Qazvin, Iran*
[4] *Department of Mechanical Engineering, Shahid Chamran University of Ahvaz, Ahvaz, Iran*

Abstract

This paper analyzes the nonlinear coupled torsional-radial vibration of single-walled carbon nanotubes (SWCNTs) based on numerical methods. Two partial differential equations that govern the nonlinear coupled torsional-radial vibration for such nanotube are derived using doublet mechanics (DM) principles. First, these equations are reduced to ordinary differential equations using Galerkin method and then solved using homotopy perturbation method (HPM) to obtain the nonlinear natural frequencies in coupled torsional-radial vibration mode. It is found that the obtained frequencies are complicated due to coupling between two vibration modes. The dependence of boundary conditions, vibration modes and nanotubes geometry on the nonlinear coupled torsional-radial vibration characteristics of SWCNTs are studied in details. It was shown that boundary conditions and maximum vibration velocity have significant effects on the nonlinear coupled torsional-radial vibration response of SWCNTs. It was also seen that unlike the linear model, as the maximum vibration velocity increases, the natural frequencies of vibration increase too. To show the effectiveness and ability of this method, the results obtained with the present method are compared with the fourth order Runge-Kuta numerical results and good agreement is observed. To the knowledge of authors, the results given herein are new and can be used as a basic work for future papers.

Keywords: homotopy perturbation method; nonlinear coupled torsional-radial vibration; single-walled carbon nano-tubes; natural frequency;

Introduction

It is known that the mechanical behavior of structures is divided in two general categories depending on whether the material phases are distributed continuously or discretely. If distribution be continuous, theories are based on classical continuum mechanics (CCM) and don't contain any scaling effects. This feature normally is the most important limitation of CCM and analyzed by many researchers [1-15]. Because of nanoscale dimensions of carbon nanotubes (CNTs), it is hard to implement accurate experiments to obtain the properties of a CNT [16, 17]. On the other hand, atomistic methods like molecular mechanics [18-21] take too

* Corresponding author: ebrahimian.reza@gmail.com

times and also are costly and time-consuming to implement especially for the systems have large scales.

Most popular approaches to simulate micromechanics the nonlocal theory [22-24], stress couple theory [6], strain gradient theory [7, 14, 15] and stress-driven theory [25-27]. For example in nonlocal elasticity, it is assumed that the stress tensor at a point is a function of strains at all points in the continuum[28]. It is different from the classical continuum theory in that the latter is based on constitutive relations which state that the stress at a point is a function of strain at that particular point [1].The nonlocal theory is deductive, in the sense that it employs field variables of intrinsic macroscopic nature (i.e., the strain and stress tensors), without explicit connections with the underlying discrete material microstructure [29]. Also, the total number of elastic macro-constants in the nonlocal theory is considerably large [2]. Mahdavi Adeli *et al*. [23] studied free torsional vibration behavior of a nonlinear nano-cone, based on the nonlocal strain gradient elasticity theory. Also, Shishesaz and Hosseini [14] investigated the mechanical behavior of a functionally graded nano-cylinder under a radial pressure using strain gradient theory.

Another popular theory for analyzing CNTs is molecular dynamics (MD). Applying MD, every single atom or molecule in CNTs is seen as a discrete mass point and the bonding forces between each pair of neighboring atoms obey Newton's laws of motion [2]. This model usually employs simplifications, such as regularity of particle distribution, symmetry and periodicity [30]. MD simulations are suitable for small scale systems and for short time intervals [31].

In order to overcome to the following limitations, various important modifications to CCM, known as higher order gradient continuum theories, were suggested to enter micro-structural features into the theory. One particular theory that has recently been applied to materials with micro-structure is doublet mechanics (DM). This theory originally developed by Granik (1978), has been applied to granular materials by Ferrari et al. [2]. In DM micro-mechanical models, solids are represented as arrays of points, particles or nodes at finite distances. This theory has shown good promise in predicting observed behaviors that are not predictable using continuum mechanics like Flamant paradox and also dispersive wave propagation.

Carbon nanotubes (CNTs) invented by Iijima [32], have many exclusive and fascinating properties. With rapid development in nanotechnology, CNT have great potential for broad applications as components in nano-electronic-mechanical systems (NEMS) which received increasing interest lately. The SWCNTs usually are subjected to complex and heavy dynamic loadings caused by different sources. By producing different states of stress, these loads might result in excess vibrations. The vibrations of SWCNTs extensively disrupt the normal performance of the system and may result to failures in some cases [33]. Due to the excellent features and huge applications of CNTs, the precise prediction of the dynamic behavior of such systems is vital. Then, any suggested models should contain the real dynamic behaviors of the system. Two important forms of vibrations that have been identified for SWCNTs are axial and torsional vibrations. For example, for the flexible CNT with long distance between supports and high flexibility its torsional vibrations are much significant. Furthermore, for determining the diameter of the CNTs and also in Raman spectra, the radial vibration must be considered. Then, it is essential to considering the coupling effect between radial and torsional vibration of a SWCNT, especially for studying stability conditions of CNTs. It can be seen from the previous works on the vibration of SWCNTs that most of existing SWCNTs systems have focused on the bending [28, 34-36], torsional [29, 37-39], radial [40, 41] or longitudinal [30, 31, 42] vibrations behavior of the shafts, solely and the coupling effect between the vibrational

modes were ignored. The coupled vibration of SWCNTs is an interesting subject because of the complexity of the equations and the analytical solutions are difficult to obtain.

Single-walled carbon nanotubes (SWCNTs) are tiny cylinders made from carbon [18]. A SWCNT can be described as a single layer of a graphite crystal that is rolled up into a seamless circular cylinder, one atom thickness, usually with a small number of carbon atoms along the circumference and a long length along the cylinder axis[43]. The radial vibration is the characteristic phonon mode of SWCNTs which leads to a periodic increase and decrease of the tube diameter[44]. In the radial vibration, all carbon atoms move coherently in the radial direction creating a breathing-like vibration of the entire tube[44, 45] [e]. This feature is specific to CNTs and is not observed in other carbon systems such as graphite[45]. The radial frequency is usually the strongest feature in SWCNT Raman spectra which plays a crucial role in the experimental determination of the geometrical properties of SWCNTs[43, 45]. Radial frequencies are very useful for identifying a given material containing SWCNTs, through the existence of radial vibration modes, and for characterizing the nanotube diameter distribution in the sample through inverse proportionality of the radial frequency to the tube diameter[43]. Therefore, it is very important to know the behavior of radial frequency of different nanotubes, precisely.

On the other hands, torsional deformation and vibration are easily seen in nano-electro-mechanical systems. For efficient design of such devices, the torsional dynamics of the nano-components are vital[22].

However, most of the researches on the axial and torsional vibration of CNTs have been limited to the linear theory and the nonlinear regime is not considered yet. The coupled vibration of SWCNTs is an interesting subject because of the complexity of the equations and the analytical solutions are difficult to obtain. Among them is torsional-radial coupling in the vibrational behavior of the SWCNT system which is originated from the large deformation of the beam. The torsional-radial coupled vibration of the SWCNTs can lead to severe vibration, and this energy boosts the amplitude of the vibration and may leads to the reduction of bit life. If not taken into consideration, the effect of coupled vibration can not only reduce the calculation accuracy, but also lose some important characteristics of the CNTs. Therefore, it is important to establish an accurate model for dynamic characteristics of the coupled vibrations of CNTs. For the case of coupled torsional-radial vibrations of the SWCNT, some nonlinearity can affect the total response of the system. It should be noted that in the linear analysis, torsional and radial vibrations are decoupled and can be studied separately. The HPM as an efficient semi-analytical approach introduced by He [46-50] for solving different linear and especially nonlinear engineering problems such as eigen value problems. In HPM, it is considered the solution as sum of a series with infinite terms so that less than three sentences result to good accuracy of the solution with rapid convergence. The series used in HPM is different from Taylor series as it contains functions rather than terms as is in Taylor series. The method can be applied to a wide class of integral and differential equations, deterministic and stochastic problems, linear and nonlinear equations. The main advantages of this method to the other methods are simplicity, high convergence, more accurate results and time saving especially in the nonhomogeneous and nonlinear equations. The HPM was also applied to study nonlinear equations appear in science and engineering problems [51-54].

To the best knowledge of authors, considering geometric nonlinearity effects along with the coupling of the torsional-radial vibrations on the dynamic behavior of the SWCNTs is not studied yet and the present paper tries to consider such analysis. Considering the complexity of the practical dynamics of the SWCNT systems, the main purpose of this study is investigating

and modeling a mechanism for the coupled nonlinear torsional-radial vibration of the SWCNTs. Another goal of this paper is to show the effectiveness of HPM and its ability and also handling the nonlinear coupled torsional-radial vibration to obtain the nonlinear frequency. The structure of the paper is as follows. In Section 2, a brief review to derive the nonlinear equation of motion for coupled torsional-radial vibration of SWCNTs is given using nonlocal theory. In Section 3, the equation of motion for SWCNTs in torsional-radial vibration is solved using HPM and the natural frequencies are obtained. The obtained nonlinear natural frequencies are compared with numerical results in Section 4 to illustrate the ability and accuracy of the proposed method. In Section 5 a brief discussion and conclusions follows.

Derivation of nonlinear equation of motion for coupled torsional-radial vibration of SWCNTs using DM

DM is a micro-mechanical theory based on a discrete material model whereby solids are represented as arrays of points or nodes at finite distances. A pair of such nodes is referred to as a doublet, and the nodal spacing distances introduce length scales into the micro-structural theory. Each node in the array is allowed to have a translation and rotation, and increments of these variables are expanded in a Taylor series about the nodal point. The order at which the series is truncated defines the degree of approximation employed. The lowest order case using only a single term in the series will not contain any length scales, while using more than one term will produce a multi length scale theory. This allowable kinematics develops micro-strains of elongation, shear and torsion (about the doublet axis). Through appropriate constitutive assumptions, these micro-strains can be related to corresponding elongational, shear and torsional micro-stresses. A pair of such particles represents a doublet as shown in Fig. 1. Corresponding to the doublet *(A, B)* there exist a doublet or branch vector ζ_a connecting the adjacent particle centers and defining the doublet axis. The magnitude of this vector $\eta_a = |\zeta_a|$ is simply the particle diameter for particles in contact. However, in general the particles need not be in contact, and for this case the length scale η_a could be used to represent a more general micro-structural feature. For example, the internal characteristic scale for the crystal lattice parameter of carbon is $\eta_a = 0.1421nm$ [1].

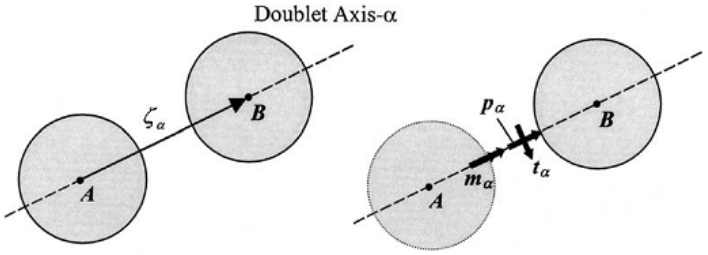

Fig. 1 doublet [2].

As mentioned, the kinematics allow relative elongational, shearing and torsional motions between the particles, and this is used to develop an elongational micro-stress p_a, shear micro-stress t_a, and torsional micro-stress m_a as shown in Fig. 1. It should be pointed out that these micro-stresses are not second order tensors in the usual continuum mechanics sense. Rather, they are vector quantities that represent the elastic micro-forces and micro-couple of interactions between doublet particles. Their directions are dependent on the doublet axes which are determined by the material micro-structure. These micro-stresses are not continuously distributed but rather exist only at particular points in the medium being simulated by DM.

From Fig. 2, suppose doublet (a, b_α) converts to doublet (a', b_α') because of kinematic translation. The superscript 0 for vectors indicates the initial state.

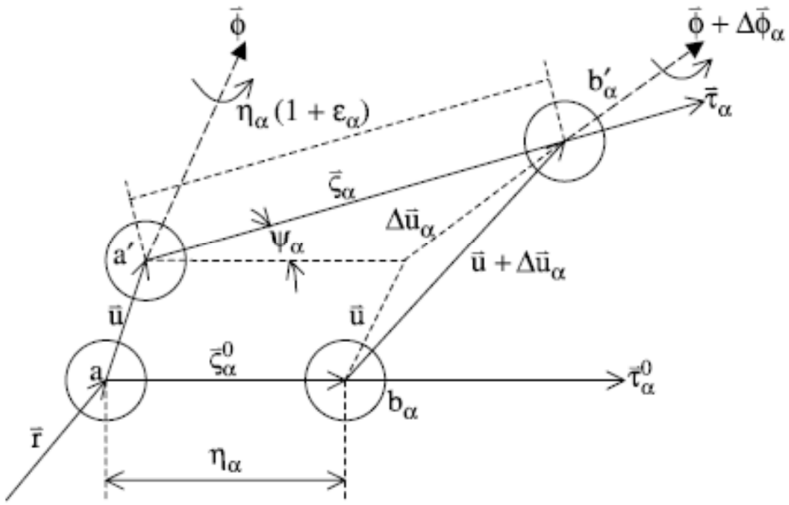

Fig. 2 Translations of the doublet nodes $a \in A$, $b_\alpha \in B_\alpha$ [2]

If $\boldsymbol{u}(\boldsymbol{x},t)$ is the displacement field coinciding with a particle displacement, then the incremental displacement is written as:

$$\Delta\boldsymbol{u}_\alpha = \boldsymbol{u}\left(\boldsymbol{x}+\boldsymbol{\zeta}^0_\alpha, t\right) - \boldsymbol{u}(\boldsymbol{x},t) \tag{1}$$

wherein, $\boldsymbol{x}$ is the position vector of particle.

The incremental function in Eq. (1) could be expanded in a Taylor series as [2]:

$$\Delta\boldsymbol{u}_\alpha = \sum_{\chi=1}^{M} \frac{(\eta_\alpha)^\chi}{\chi!}\left(\boldsymbol{\tau}^0_\alpha.\boldsymbol{\nabla}\right)^\chi \boldsymbol{u} \tag{2}$$

wherein $\boldsymbol{\nabla}$ is the Del operator in general coordinates and η is the internal characteristic length scale. As mentioned above, the number of terms used in the series expansion of the local deformation field determines the order of the approximation in DM.

Here, $\alpha = 1,...,n$ while *n* is referred to the numbers of doublets. For the problem under study, it is assumed that the shear and torsional micro-deformations and micro-stresses are negligible and thus only extensional strains and stresses exist.

The extensional micro-strain scalar measure ϵ_α, representing the axial deformation of the doublet vector, is defined as [2]:

$$\epsilon_\alpha = \frac{\boldsymbol{\tau}_\alpha.\Delta\boldsymbol{u}_\alpha}{\eta_\alpha} \tag{3}$$

From Fig. 1, it can be written that

$$\boldsymbol{\tau}_\alpha = \frac{1}{1+\epsilon_\alpha}\left(\boldsymbol{\tau}^0_\alpha + \frac{\Delta\boldsymbol{u}_\alpha}{\eta_\alpha}\right) \tag{4}$$

As in linear elasticity, it is assumed that the relative displacement $|\Delta\boldsymbol{u}_\alpha|$ is small compared to the doublet separation distance η_α ($|\Delta\boldsymbol{u}_\alpha| \ll \eta_\alpha$) so that it may be assumed that $\boldsymbol{\tau}_\alpha = \boldsymbol{\tau}^0_\alpha$. In

nonlinear elasticity $\boldsymbol{\tau}_\alpha \neq \boldsymbol{\tau}_\alpha^0$ and the following approximate relations between $\boldsymbol{\tau}_\alpha$ and $\boldsymbol{\tau}_\alpha^0$ are present [31]:

$$\boldsymbol{\tau}_\alpha.\boldsymbol{\tau}_\alpha^0 = \cos(\psi_\alpha) = 1 - \frac{\psi_\alpha^2}{2} \tag{5}$$

$$\boldsymbol{\tau}_\alpha \times \boldsymbol{\tau}_\alpha^0 = \sin(\boldsymbol{\psi}_\alpha) = \boldsymbol{\psi}_\alpha \tag{6}$$

wherein ψ_α is the angle between initial and current branch vectors.

From Eq. (4)- (6), ψ_α^2 can be obtained as follow

$$\psi_\alpha^2 = \frac{1}{\eta_\alpha^2\left(1+2\epsilon_\alpha+\epsilon_\alpha^2\right)}\left(\Delta\boldsymbol{u}_\alpha \times \boldsymbol{\tau}_\alpha^0\right).\left(\Delta\boldsymbol{u}_\alpha \times \boldsymbol{\tau}_\alpha^0\right) \tag{7}$$

If ψ_α^2 obtained from Eq. (7) is substituted in Eq. (3), it can be concluded that

$$\frac{1}{\eta_\alpha^2\left(1+2\epsilon_\alpha+\epsilon_\alpha^2\right)}\left(\Delta\boldsymbol{u}_\alpha \times \boldsymbol{\tau}_\alpha^0\right).\left(\Delta\boldsymbol{u}_\alpha \times \boldsymbol{\tau}_\alpha^0\right) = 2 - \frac{2}{1+\epsilon_\alpha}\left(1+\frac{\Delta\boldsymbol{u}_\alpha.\boldsymbol{\tau}_\alpha^0}{\eta_\alpha}\right) \tag{8}$$

With solving this equation, the micro-strain for nonlinear approximation can be obtained. It is clear that for linear approximation that $\Delta\boldsymbol{u}_\alpha \times \boldsymbol{\tau}_\alpha^0 = 0$ and then the linear approximation can be obtained. Multiplication both side of Eq. (8) with $\frac{1}{2}\left(1+2\epsilon_\alpha+\epsilon_\alpha^2\right)$ yields

$$\frac{1}{2\eta_\alpha^2}\left(\Delta\boldsymbol{u}_\alpha \times \boldsymbol{\tau}_\alpha^0\right).\left(\Delta\boldsymbol{u}_\alpha \times \boldsymbol{\tau}_\alpha^0\right) + \left(1+\epsilon_\alpha\right)\left(1+\frac{\Delta\boldsymbol{u}_\alpha.\boldsymbol{\tau}_\alpha^0}{\eta_\alpha}\right) = 1+2\epsilon_\alpha+\epsilon_\alpha^2 \tag{9}$$

In Eq. (9), ignoring ϵ_α^2 in comparison with ϵ_α and $\epsilon_\alpha \frac{\Delta u_{\alpha i}\tau_{\alpha i}^0}{\eta_\alpha}$ in comparison with $\frac{\Delta u_{\alpha i}\tau_{\alpha i}^0}{\eta_\alpha}$, gives the following approximate nonlinear micro-strain-displacements equation as

$$\epsilon_\alpha = \frac{\Delta\boldsymbol{u}_\alpha.\boldsymbol{\tau}_\alpha^0}{\eta_\alpha} + \frac{1}{2\eta_\alpha^2}\left(\Delta\boldsymbol{u}_\alpha \times \boldsymbol{\tau}_\alpha^0\right).\left(\Delta\boldsymbol{u}_\alpha \times \boldsymbol{\tau}_\alpha^0\right) \tag{10}$$

One may write $\boldsymbol{\tau}_\alpha^0 = \tau_{\alpha j}^0 \boldsymbol{e}_j$ where $\tau_{\alpha j}^0$ are the cosines of the angles between the directions of micro-stress and the coordinates and $\boldsymbol{e}_i$ is the unit vector in Cartesian coordinate. Setting $\boldsymbol{\tau}_\alpha^0 = \tau_{\alpha i}^0 \boldsymbol{e}_i$, $\Delta\boldsymbol{u}_\alpha = \Delta u_{\alpha i}\boldsymbol{e}_i$ in Eq. (10), it is concluded that

$$\epsilon_\alpha = \frac{1}{2\eta_\alpha^2}\left(\Delta u_{\alpha i}\Delta u_{\alpha i}\tau_{\alpha j}^0\tau_{\alpha j}^0 - \Delta u_{\alpha i}\Delta u_{\alpha j}\tau_{\alpha i}^0\tau_{\alpha j}^0\right) + \frac{\Delta u_{\alpha i}\tau_{\alpha i}^0}{\eta_\alpha} \tag{11}$$

In DM under such assumptions and neglecting temperature effect, the relation between micro-strain and micro-stress is written in the below [36].

$$p_\alpha = \sum_{\beta=1}^{n} A_{\alpha\beta}\epsilon_\beta \tag{12}$$

Where in p_α is axial micro-stress along doublet axes. An example of the axial micro-stress is the interatomic forces between atoms or molecules located at the nodes of a general array such as a crystalline lattice. In the case of linear and homogeneous inter nodal central interactions. Eq. (12) can be interpreted as the constitutive equation in the linear and homogeneous DM and $A_{\alpha\beta}$ is the matrix of the micro-modules of the doublet.

In the homogeneous and isotropic media with local interaction the above relation is simplified as below [41]:

$$p_\alpha = A_0\epsilon_\alpha \tag{13}$$

The relation between micro-stresses and macro-stresses is [2, 33]:

$$\boldsymbol{\sigma}^{(M)} = \sum_{\alpha=1}^{n} \boldsymbol{\tau}_\alpha^0 \boldsymbol{\tau}_\alpha^0 \sum_{\chi=1}^{M} \frac{(-\eta_\alpha)^{\chi-1}}{\chi!} \left(\boldsymbol{\tau}_\alpha^0.\nabla\right)^{\chi-1} p_\alpha \tag{14}$$

In the above equation, M is the degree of approximation which in the series is truncated. Substituting Eq. (11) into Eq. (13) and the result into Eq. (14) and neglecting scale effect yields

$$\sigma_{mn} = A_0\tau_{\alpha m}^0\tau_{\alpha n}^0\left[\frac{\Delta u_{\alpha i}\tau_{\alpha i}^0}{\eta_\alpha} + \frac{1}{2\eta_\alpha^2}\left(\Delta u_{\alpha i}\Delta u_{\alpha i}\tau_{\alpha j}^0\tau_{\alpha j}^0 - \Delta u_{\alpha i}\Delta u_{\alpha j}\tau_{\alpha i}^0\tau_{\alpha j}^0\right)\right] \tag{15}$$

This equation is the relation between macro-stresses and displacements in nonlinear regime. Now, the form of matrix $[\boldsymbol{A}]$ in Eq. (12) containing elastic macro-constant for plane problem (two-dimensional) is obtained. For this reason, consider Fig. 3. According to Fig. 3, in the $x_1 - x_2$ plane, there are only three doublets with equal angels between them. The solution for the scale less condition can be calculated directly from the associated CCM problem for an isotropic material. For the plane problems in the homogeneous media, $[\boldsymbol{A}]$ is a symmetric matrix of order 3 with the most general form [20] as follow:

$$A = \begin{bmatrix} a & b & b \\ b & a & b \\ b & b & a \end{bmatrix} \tag{16}$$

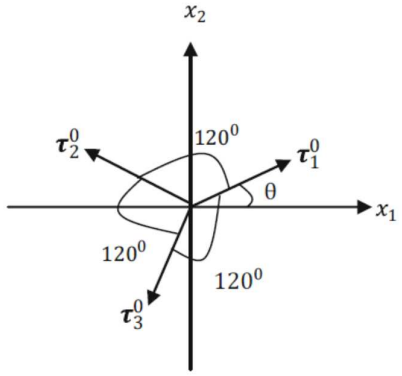

Fig. 3 Three doublets with equal angle 120^0 between them [1]

It can be shown that for any θ, if Eq. (16) is substituted into Eq. (12) and plane stress condition is considered, the coefficients a and b in matrix A are found to be [2]:

$$a=\frac{4}{9}\mu\frac{7\lambda+10\mu}{\lambda+2\mu},\ b=\frac{4}{9}\mu\frac{\lambda-2\mu}{\lambda+2\mu} \tag{17}$$

where λ,μ are Lame's constants and can be written in term of elasticity modulus *E*, Poisson ratio ν and shear modulus *G* as below [30]:

$$\lambda=\frac{\nu E}{(1+\nu)(1-2\nu)},\mu=G=\frac{E}{2(1+\nu)} \tag{18}$$

One could use $b=0$ as a quantitative guide to the applicability of the simpler constitutive relations such as Eq. (13). If $\lambda=2\mu$ (or $\nu=\frac{1}{3}$) in plane stress condition from Eq. (18), it is concluded that $b=0$ and

$$a=A_0=\frac{8\mu}{3}=E \tag{19}$$

Now, the coupled torsional-radial governing differential equations of motion representing the vibrational behavior of the SWCNTs are derived in this section. The shell theory is employed and the effects of rotary inertia and gyroscopic moments are neglected. Furthermore, the radial, axial and torsional deformations are taken into account, and it is assumed that the amplitude of the vibration is large, and stretching nonlinearity which is originated from the extension of the shaft centerline is considered. A shell is a three-dimensional body whose boundary surface has special features. Before describing such a body, it is convenient to introduce suitable coordinate systems. Let the points of a region *R* in a Euclidean 3-space be referred to a fixed right-handed rectangular Cartesian coordinate system $x_i\,(i=1,2,3)$ and let $(\theta_1,\theta_2,\theta_3)$ be a general curvilinear system defined by the transformation relations [38]:

$$x_i=x_i(\theta_1,\theta_2,\theta_3) \tag{20}$$

The physical components of stress resultants known as $N_{\alpha i}$ in curvilinear coordinate are given by [17]

$$\frac{1}{a_1a_2}\left[(a_2N_{11})_{,1}+(a_2N_{11})_{,2}+a_{1,2}N_{12}-a_{2,1}N_{22}\right]+\frac{N_{13}}{r_1}+\rho f_1=\rho\frac{\partial^2u_1}{\partial t^2} \tag{21}$$

$$\frac{1}{a_1a_2}\left[(a_2N_{12})_{,1}+(a_1N_{22})_{,2}+a_{1,2}N_{11}-a_{2,1}N_{21}\right]+\frac{N_{23}}{r_2}+\rho f_2=\rho\frac{\partial^2u_2}{\partial t^2} \tag{22}$$

$$\frac{1}{a_1a_2}\left[(a_2N_{13})_{,1}+(a_1N_{23})_{,2}\right]+\left(\frac{N_{11}}{r_1}+\frac{N_{22}}{r_2}\right)+\rho f_3=\rho\frac{\partial^2u_3}{\partial t^2} \tag{23}$$

wherein r_1 and r_2 are the radii of curvature of the surface, a_1 and a_2 are the magnitudes of the surface base vectors and f_i are body forces.

The physical components of moment resultants known as $N_{\alpha i}$ in curvilinear coordinate are given by [1]:

$$\frac{1}{a_1a_2}\left[(a_2M_{11})_{,1}+(a_2M_{11})_{,2}+a_{1,2}M_{12}-a_{2,1}M_{22}\right]+\frac{M_{13}}{r_1}+\rho\bar{l_1}=N_{13} \tag{24}$$

$$\frac{1}{a_1a_2}\left[(a_2N_{12})_{,1}+(a_1N_{22})_{,2}+a_{1,2}N_{11}-a_{2,1}N_{21}\right]+\frac{N_{23}}{r_2}+\rho\bar{l_2}=N_{23} \tag{25}$$

$$\frac{1}{a_1a_2}\left[(a_2M_{13})_{,1}+(a_1M_{23})_{,2}\right]-\left(\frac{M_{11}}{r_1}+\frac{M_{22}}{r_2}\right)+\rho\bar{l_3}=N_{23} \tag{26}$$

Eqs. (21)– (26) are the governing equations for thin shells in general curvilinear coordinates. Now, consider a SWCNT of length *L*, mean radius *R*, Young's modulus *E*, Poisson's ratio ν and mass density ρ as shown in Fig. 4. In cylindrical coordinate, the coordinate components become

$$\theta_1 = z, \theta_1 = \theta, \theta_1 = r \tag{27}$$

The radii of curvature and the coefficients a_1 and a_2 in the cylindrical coordinates are written respectively, as

$$r_1 = \infty, r_2 = r, a_1 = 1, a_2 = r \tag{28}$$

The orthogonal axes of coordinate system (r, θ, z) correspond to the normal, tangent and binormal (axial) axes in local cylindrical system of coordinates, respectively. The displacements of the center of a sample element along the normal, tangent and binormal axes are demonstrated by u_r, u_θ and u_z correspondingly and the torsional deformation of the cross section is denoted by θ around the *x* direction. Here, the radial deformations and torsional warping are also added to the theory. Substitution of Eq. (27) and (28) into Eq. (21)– (26) yields

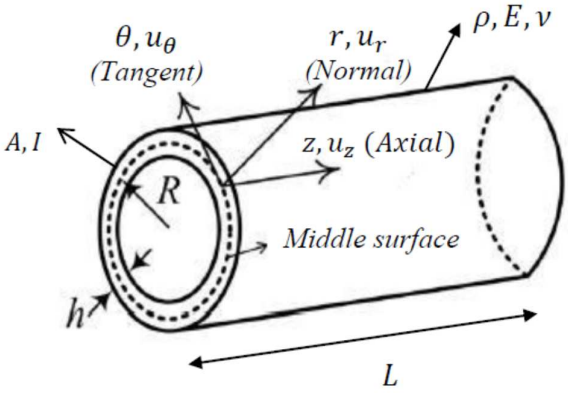

Fig. 4 A nanotube in cylindrical coordinate.

$$\frac{\partial N_{zz}}{\partial z} + \frac{1}{r}\frac{\partial N_{\theta z}}{\partial \theta} + \rho f_z = \rho \frac{\partial^2 u_z}{\partial t^2} \tag{29}$$

$$\frac{\partial N_{z\theta}}{\partial z} + \frac{1}{r}\frac{\partial N_{\theta\theta}}{\partial \theta} + \frac{N_{\theta r}}{r} + \rho f_\theta = \rho \frac{\partial^2 u_\theta}{\partial t^2} \tag{30}$$

$$\frac{\partial N_{zr}}{\partial z} + \frac{1}{r}\frac{\partial N_{\theta r}}{\partial \theta} - \frac{N_{\theta\theta}}{r} + \rho f_r = \rho \frac{\partial^2 u_r}{\partial t^2} \tag{31}$$

$$\frac{\partial M_{zz}}{\partial z} + \frac{1}{r}\frac{\partial M_{\theta z}}{\partial \theta} + \rho \bar{l_z} = N_{zr} \tag{32}$$

$$\frac{\partial M_{z\theta}}{\partial z} + \frac{1}{r}\frac{\partial M_{\theta\theta}}{\partial \theta} + \frac{1}{r}M_{\theta r} + \rho \bar{l_\theta} = N_{\theta r} \tag{33}$$

$$\frac{M_{zr}}{\partial z} + \frac{1}{r}\frac{M_{\theta r}}{\partial \theta} - \frac{M_{\theta\theta}}{r} + \rho \bar{l_r} = N_{rr} \tag{34}$$

Eqs. (29) - (34) are the equations of motion of a thin shell in the cylindrical coordinates and should be solved in order to develop the dynamic analysis of the system. N_{ij} and M_{ij} are resultant forces and resultant moments, respectively and are written with the following equations:

$$N_{ij} = \int_{-\frac{h}{2}}^{\frac{h}{2}} \sigma_{ij}^{(M)} dr \ , i, j = 1,2,3 \tag{35}$$

$$M_{ij} = \int_{-\frac{h}{2}}^{\frac{h}{2}} z\sigma_{ij}^{(M)} dr \ , i, j = 1,2,3 \tag{36}$$

It should be noted that SWCNTs are essentially two-dimensional. So introducing of the stresses and displacements in SWCNT considered as a three-dimensional solid seems a bit artificial. But nevertheless, Eqs. (29) – (34) are still valid since these equations describe an equilibrium state of a shell characterized by stress resultants and moment resultants.

In this study, the following assumptions, known as Love's first approximation, for cylindrical shells are made [39]:

1. All points that lie on a normal to the middle surface before deformation do the same after the deformation. Then the transverse shear stresses $\sigma_{rz}^{(M)}$ and $\sigma_{\theta z}^{(M)}$ are assumed to be negligible.
2. Displacements are small compared to the shell thickness.
3. The normal stresses in the thickness direction ($\sigma_{rr}^{(M)}$) are negligible (planar state of stress).

Assuming axisymmetric and homogeneity for the entire tube and that the nanotube vibrates in radial and torsional modes only such that the cross-section of the tube is not elastically deformed and also neglecting body forces, it may be concluded

$$\frac{\partial}{\partial \theta} = \frac{\partial}{\partial \mathrm{r}} = 0, u_z = 0 \tag{37}$$

Under such assumptions, Eqs. (29)- (34) are reduced to

$$\frac{\partial N_{z\theta}}{\partial z} = \rho \frac{\partial^2 u_\theta}{\partial t^2} \tag{38}$$

$$-\frac{N_{\theta\theta}}{r} = \rho \frac{\partial^2 u_r}{\partial t^2} \tag{39}$$

which are the equations of motion for coupled torsional-radial vibration of SWCNTs.

The nonlinear strain-displacement relation is written [31]:

$$\boldsymbol{\varepsilon} = \frac{1}{2}\left(\nabla \boldsymbol{u} + \nabla \boldsymbol{u}^T + \nabla \boldsymbol{u}^T \nabla \boldsymbol{u}\right) \tag{40}$$

where $\boldsymbol{\nabla}$ is the gradient operator in cylindrical coordinates given as

$$\nabla = \frac{\partial}{\partial r}\boldsymbol{e}_r + \frac{1}{r}\frac{\partial}{\partial \theta}\boldsymbol{e}_\theta + \frac{\partial}{\partial z}\boldsymbol{e}_z \tag{41}$$

$\nabla \boldsymbol{u}$ can be written in cylindrical coordinate as [55]:

$$\boldsymbol{\nabla u} = \begin{bmatrix} \frac{\partial u_r}{\partial r} & \frac{1}{r}\left(\frac{\partial u_r}{\partial \theta} - u_\theta\right) & \frac{\partial u_r}{\partial z} \\ \frac{\partial u_\theta}{\partial r} & \frac{1}{r}\left(\frac{\partial u_\theta}{\partial \theta} + u_r\right) & \frac{\partial u_\theta}{\partial z} \\ \frac{\partial u_z}{\partial r} & \frac{1}{r}\frac{\partial u_z}{\partial \theta} & \frac{\partial u_z}{\partial z} \end{bmatrix} \tag{42}$$

Substituting Eq. (42) into Eq. (40) and making some manipulations, yields

$$\varepsilon_{z\theta} = \frac{1}{2}\left[2\frac{\partial u_\theta}{\partial z} - \frac{u_\theta}{r}\frac{\partial u_r}{\partial z} + \frac{u_r}{r}\frac{\partial u_\theta}{\partial z} \right] \tag{43}$$

$$\varepsilon_{\theta\theta} = \frac{1}{2}\left[2\frac{u_r}{r} + \frac{u_\theta^2}{r^2} + \frac{u_r^2}{r^2} \right] \tag{44}$$

Now, substituting Eq. (43) and (44) into Eq. (15) along with using Eq. (42) and the results into Eq. (38) and (39) with making some manipulations with neglecting scale effect yields

$$Gh\left[\frac{\partial^2 u_\theta}{\partial z^2} + \frac{1}{2r}\left(u_r \frac{\partial^2 u_\theta}{\partial z^2} - u_\theta \frac{\partial^2 u_r}{\partial z^2} \right) \right] = \rho h \frac{\partial^2 u_\theta}{\partial t^2} \tag{45}$$

$$-\frac{1}{r}\frac{E}{1-\nu^2} h\left[\frac{u_r}{r} + \frac{1}{2r^2}\left(u_r^2 + u_\theta^2 \right) \right] = \rho h \frac{\partial^2 u_r}{\partial t^2} \tag{46}$$

Eq. (45) and (46) are the equations of motion in nonlinear coupled torsional-radial vibration of SWCNTs. From these equations, it can be concluded that because of nonlinear terms, the two equations are coupled with together. The fundamental linear equations can be simply calculated by setting the nonlinear terms to zero. In this case, the two equations will be decoupled.

Application of HPM for solving nonlinear vibrations of SWCNTs

In this section, the nonlinear governing equations for the coupled torsional-radial vibration of SWCNTs are solved. The deflection of the nanotube is subjected to the following boundary conditions in radial and torsional direction, respectively.

For two clamped (C-C) boundary conditions

$$u_\theta(\mathrm{z},t) = 0 \;\; at \;\; \mathrm{z} = 0, L \tag{47}$$

For two free (F-F) boundary conditions

$$\frac{\partial u_\theta(\mathrm{z},t)}{\partial z} = 0 \, at \;\; \mathrm{z} = 0, L \tag{48}$$

For clamped-free (C-F) boundary condition

$$u_\theta(\mathrm{z},t) = 0 \, at \;\; \mathrm{z} = 0, \frac{\partial u_\theta(\mathrm{z},t)}{\partial z} = 0 \, at \;\; \mathrm{z} = L \tag{49}$$

Table1. Common boundary conditions for the torsional direction

End conditions of beam	Mode shape (normal function)
Two clamped (C-C)	$sin\left(\frac{n\pi}{L}z\right)$
Two free (F-F)	$cos\left(\frac{n\pi}{L}z\right)$
clamped-free (C-F)	$1-cos\left(\frac{2n\pi}{L}z\right)$

In mathematics, in the area of numerical analysis, Galerkin methods are a class of methods for converting a continuous operator problem such as a differential equation to a discrete problem. Indeed, it is equivalent of applying the variation of parameters method to a function space, by

converting the equation to a weak formulation. A key feature of this method is that they rely on integrals of functions that can readily be evaluated on domains of essentially arbitrary shape. Galerkin's method provides powerful numerical solution to differential equations and modal analysis. Now, the nonlinear equations of motion are solved to obtain the nonlinear natural frequencies. The separation of variables is used and assumed that $u_\theta(z,t)=\varphi(z)U(t)$ and $u_z(z,t)=\psi(z)W(t)$ where $\varphi(z)$ and $\psi(z)$ are the eigenmodes of the tube satisfying the kinematic boundary conditions and $U(t)$ and $W(t)$ the time-dependent deflection parameter of the nanotube, respectively. The base functions corresponding to the above boundary conditions are given in Table 1 for torsional mode.

Applying the Galerkin method, the governing equations of motion are obtained as follows:

$$G\left[a_1U+\frac{1}{2r}(a_2+a_3)UW\right]=\rho a_4\frac{\partial^2U}{\partial t^2} \tag{50}$$

$$\frac{E}{1-\nu^2}\left[a_5W+\frac{1}{2r}a_6W^2+\frac{1}{2r}a_7U^2\right]=\rho r^2a_8\frac{\partial^2W}{\partial t^2} \tag{51}$$

The above equations are the differential equations of motion governing the nonlinear coupled torsional-radial vibrations of SWCNTs subjected to the following initial conditions:

$$U(0)=0,\frac{dU}{dt}(0)=U_{max} \tag{52}$$

$$W(0)=0,\frac{dW}{dt}(0)=W_{max} \tag{53}$$

wherein U_{max} and W_{max} denote the maximum velocities of oscillation in circumferential and radial directions, respectively. In Eqs. (50) and (51), $\alpha_1,\alpha_2,...,\alpha_8$ are as follows:

$$\alpha_1=\int_0^L\varphi''(z)\varphi(z)dz,\alpha_2=\int_0^L\varphi''(z)\psi(z)\varphi(z)dz,\alpha_3=-\int_0^L\psi''(x)\varphi^2(z)dz,\alpha_4=\int_0^L\varphi^2(z)dz \tag{54}$$

$$\alpha_5=-\int_0^L\psi^2(z)dz,\alpha_6=-\int_0^L\psi^3(z)dz,\alpha_7=-\int_0^L\psi(z)\varphi^2(z)dz,\alpha_8=\int_0^L\psi^2(z)dz \tag{55}$$

Changing the variable $\tau=\omega t,\nu=\Omega t,a=\frac{U}{r},b=\frac{W}{r}$ and $r=\sqrt{\frac{I}{A}}$, Eqs. (50) and (51) can be transformed to the following nonlinear equation:

$$\omega^2\frac{d^2a}{\partial\tau^2}+Aa+Bab=0 \tag{56}$$

$$\Omega^2\frac{d^2b}{\partial\nu^2}+Cb+Db^2+Ea^2=0 \tag{57}$$

wherein ω and Ω are unknown nonlinear torsional and radial frequencies in the coupled nonlinear torsional-radial vibration of SWCNTs have to be determined. The coefficients A,B,C,D and E are defined by the following equations

$$A=-\frac{\alpha_1}{\alpha_4}\frac{G}{\rho}=\omega_L^2 \tag{58}$$

$$B=-\frac{1}{2r}\frac{\alpha_2+\alpha_3}{\alpha_4}\sqrt{\frac{I}{A}}\frac{G}{\rho} \tag{59}$$

$$C=-\frac{\alpha_5}{\alpha_8}\frac{E}{\rho\left(1-\nu^2\right)}\frac{1}{r^2}=\Omega_L^2 \tag{60}$$

$$D=-\frac{1}{2}\frac{\alpha_6}{\alpha_8}\frac{1}{2r^3}\sqrt{\frac{I}{A}}\frac{E}{\rho\left(1-\nu^2\right)} \tag{61}$$

$$E=-\frac{1}{2}\frac{\alpha_7}{\alpha_8}\frac{1}{2r^3}\sqrt{\frac{I}{A}}\frac{E}{\rho\left(1-\nu^2\right)} \tag{62}$$

In Eqs. (58) and (60), $\omega_L=\sqrt{A}$ and $\Omega_L=\sqrt{C}$ is the linear, free vibration frequency in the torsional and radial vibration modes, respectively. To determine unknown natural frequencies, New HPMs are applied to seek the solutions of Eqs. (56) and (57). The following homotopies with ω_0 and Ω_0 as the initial approximations for the angular frequencies are considered

$$\left(1-p\right)\omega_0^2\left(\frac{d^2a}{\partial\tau^2}+a\right)+p\left(\omega^2\frac{d^2a}{\partial\tau^2}+Aa+Bab\right)=0 \tag{63}$$

$$\left(1-p\right)\Omega_0^2\left(\frac{d^2b}{\partial\nu^2}+b\right)+p\left(\Omega^2\frac{d^2b}{\partial\nu^2}+Cb+Db^2+Ea^2\right)=0 \tag{64}$$

Here p is a parameter, $a=a\left(\tau,p\right)$, $b=b\left(\nu,p\right)$, $\omega=\omega\left(p\right)$ and $\Omega=\Omega\left(p\right)$. Obviously, when $p=0$, Eq. (63) and (64) yields the following linear harmonic equations

$$\frac{d^2a}{\partial\tau^2}+a=0\ ,a\left(0\right)=0\ ,\frac{da\left(0\right)}{\partial\tau}=X \tag{65}$$

$$\frac{d^2b}{\partial\nu^2}+b=0\ ,b\left(0\right)=0\ ,\frac{db\left(0\right)}{\partial\nu}=Y \tag{66}$$

It is notable that for $p=1$, it results the nonlinear Eqs. (56) and (57), respectively. As embedding parameter $p$varied from 0 to 1, the solutions $a=a\left(\tau,p\right)$ and $\omega=\omega\left(p\right)$ along with $b=b\left(\nu,p\right)$ and $\Omega=\Omega\left(p\right)$ of the homotopy Eq. (63) and (64) change from their initial approximations $a_0\left(\tau\right),\omega_0$ and $b_0\left(\nu\right),\Omega_0$ to the required solutions $a\left(\tau\right),\omega$ and $b\left(\nu\right),\Omega$ of Eq. (56) and (57), respectively. Suppose the solution of Eq. (56) and (57) to be in the following forms:

$$a\left(\tau\right)=a_0\left(\tau\right)+pa_1\left(\tau\right)+\ldots \tag{67}$$

$$\omega=\omega_0+p\omega_1+\ldots \tag{68}$$

$$b\left(\nu\right)=b_0\left(\nu\right)+pb_1\left(\nu\right)+\ldots \tag{69}$$

$$\Omega=\Omega_0+p\Omega_1+\ldots \tag{70}$$

Substituting the above relations into the Eq. (56) and (57), respectively and equaling the coefficients of the terms with equal powers of p, the following linear differential equations are obtained

$$\begin{aligned} &p^0: \frac{d^2a_0}{\partial\tau^2} + a_0 = 0\,, a_0(0) = 0\,, \frac{da_0(0)}{\partial\tau} = X \\ &p^1: \omega_0^2\left(\frac{d^2a_1}{\partial\tau^2} + a_1\right) + \left(\omega^2\frac{d^2a_0}{\partial\tau^2} + Aa_0 + Ba_0b_0\right) = 0\,, a_1(0) = 0\,, \frac{da_1(0)}{\partial\tau} = 0 \\ &\qquad\vdots \end{aligned} \tag{71}$$

$$\begin{aligned} &p^0: \frac{d^2b_0}{\partial\nu^2} + b_0 = 0\,, b_0(0) = 0\,, \frac{db_0(0)}{\partial\nu} = Y \\ &p^1: \Omega_0^2\left(\frac{d^2b_1}{\partial\nu^2} + b_1\right) + \left(\Omega^2\frac{d^2b_0}{\partial\nu^2} + Cb_0 + Db_0^2 + Ea_0^2\right) = 0\,, b_1(0) = 0\,, \frac{db_1(0)}{\partial\nu} = 0 \\ &\qquad\vdots \end{aligned} \tag{72}$$

The solution of the initial (zero) approximation is simply given by

$$a_0(\tau) = X\sin(\tau) \tag{73}$$

$$b_0(\nu) = Y\sin(\nu) \tag{74}$$

Substituting Eqs. (73) and (74) into the first approximation Eqs. (71) and (72), respectively, it is obtained that

$$\omega_0^2\left(\frac{d^2a_1}{\partial\tau^2} + a_1\right) + \left[-\omega_0^2 X\sin(\tau) + AX\sin(\tau) + BXY\sin^2(\tau)\right] = 0 \tag{75}$$

$$\Omega_0^2\left(\frac{d^2b_1}{\partial\nu^2} + b_1\right) + \left[-\Omega_0^2 Y\sin(\nu) + CY\sin(\nu) + DY^2\sin^2(\nu) + EX^2\sin^2(\nu)\right] = 0 \tag{76}$$

Expanding the trigonometric function using Fourier sine series for $\sin^2(\tau)$ in the first period yields

$$\sin^2(\tau) \cong \frac{8}{3\pi}\sin(\tau) - \frac{8}{15\pi}\sin(3\tau) \tag{77}$$

Substituting Eq. (77) into Eqs. (75) and (76) and letting the coefficient of $\sin(\tau)$ to be zero in order to eliminate the secular terms, it is found that

$$\omega = \sqrt{A + \frac{8}{3\pi}BY} \tag{78}$$

$$\Omega = \sqrt{C + \frac{8}{3\pi}\left(DY + E\frac{X^2}{Y}\right)} \tag{79}$$

It can also be seen that in contrast to linear systems, the frequencies of the vibration are dependent on its velocity amplitude which are related to the initial conditions so that the larger the amplitude, the more pronounced the discrepancy between the linear and nonlinear frequencies becomes. This is caused by the nonlinearity of the system. It should be noted that if the dependence of the frequency to amplitude of vibration is neglected the linear natural frequency of the system is obtained. The results demonstrate that the nonlinear torsional natural frequency is deviated from the linear part only by the torsional vibrations amplitude while the

nonlinear radial natural frequencies are dependent on the torsional and radial vibrations velocity of the system. Moreover, it can be seen that the torsional mode number (n) affects the torsional nonlinear natural frequency. This means that in general, different torsional mode numbers can combine to establish the nonlinear torsional natural frequency.

Considering Eqs. (78) and (79), the solution of Eqs. (75) and (76) can be obtained as

$$a_1(\tau)=\frac{3}{5}\frac{BXY}{3\pi A+8BX}\left[sin(\tau)-\frac{1}{3}sin(3\tau)\right] \tag{80}$$

$$b_1(\nu)=\frac{3}{5}\frac{DY^2+EX^2}{3\pi YC+8\left(DY^2+EX^2\right)}\left[sin(\nu)-\frac{1}{3}sin(3\nu)\right] \tag{81}$$

Thus, the first approximate solution of Eqs. (56) and (57) can be written as follows:

$$a(\tau)=a_0(\tau)+a_1(\tau)=Xsin(\tau)+\frac{3}{5}\frac{BXY}{3\pi A+8BX}\left[sin(\tau)-\frac{1}{3}sin(3\tau)\right] \tag{82}$$

$$b(\nu)=b_0(\nu)+b_1(\nu)=Ysin(\nu)+\frac{3}{5}\frac{DY^2+EX^2}{3\pi YC+8\left(DY^2+EX^2\right)}\left[sin(\nu)-\frac{1}{3}sin(3\nu)\right] \tag{83}$$

\\Now, the error analysis is discussed briefly. The numerical errors enter to the problem during Eqs. (67) - (70). Because, only two terms are considered in Eqs. (82) and (83) and only one term in Eqs. (78) and (79). It should be pointed out that the governing equation derived from the HPM principle turns out to be an infinite order series. Because it is almost impossible to analyze the infinite order series, only few terms in the infinite series in Eq. (67) - (70) are retained. It should be added that numerical are also entered to the problem during Eq. (50) and (51) which in Galerkin method is used.

Results and discussion

In order to validate the presented method, the results obtained herein using Galerkin and HPM methods are compared with the available numerical results.

To this end, in Fig. 5 nondimensional amplitude of vibration for axial and torsional modes are drawn againt the nondimensional time using fourth-order Runge-Kutta method and presented method. The sample SWCNT that has been used in this figure and upcoming figures is Zigzag (16, 0) and clamped-free boundary condition is considered for it. From this figure, the boundary condition is assumed to be clamped-free. From this figure, it can be seen that the present method predictions of the nonlinear coupled torsional-radial vibration amplitudes are in good agreement with the fourth-ordered Runge-Kuta numerical results. Now, the dependence of boundary conditions, vibration modes and nanotubes geometry on the nonlinear coupled torsional-radial vibration characteristics of SWCNTs are studied in details for Zigzag (16, 0). It should be added that one may relate the natural frequency (f) is related to the angular frequency (ω) as $f=\frac{w}{2\pi}$. This equations is used in Figs. 5- 10 to give the frequencies in *THz* .Throughout this paper, the mechanical properties of SWCNT are assumed to be: Poisson's ratio $\nu=0.2$, mass density $\rho=2300\frac{kg}{m^3}$ and Young's modulus $E=1.1TPa$ [1].

In this section, comparison between the results obtained herein using HPM and the available numerical results are presented to validate the presented method.

To demonstrate the accuracy of the obtained analytical results, the variation of nondimensional vibration amplitude for torsional mode is plotted versus the nondimensional time for Zigzag (16, 0) SWCNT using fourth-order Runge-Kutta method and the presented method in Fig. 5. From this figure, it can be seen that the HPM predictions of the nonlinear coupled torsional-radial frequencies are in good agreement with the fourth-ordered Runge-Kuta numerical results. The boundary condition is assumed to be clamped-free.

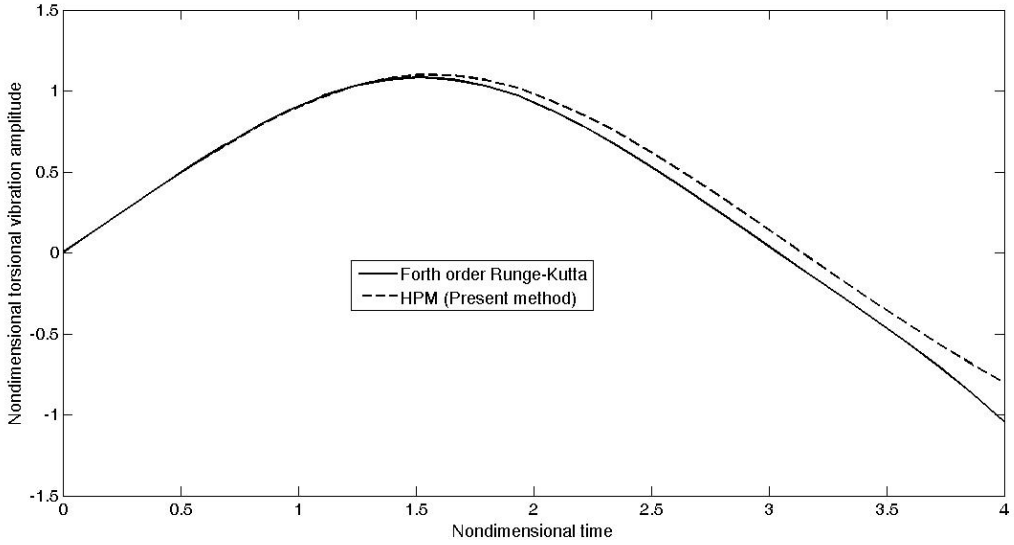

Fig. 5 Nondimensional vibration amplitudes for torsional vibration versus nondimensional time for Zigzag (16, 0) nanotube with $X = Y = 1$ for clamped-free boundary condition.

Figs. 6 and 7 show the nonlinear natural frequencies variation versus maximum torsional and radial vibration velocity for Zigzag (16, 0), respectively. As can be seen from these figures, in contrast to linear systems, the nonlinear natural frequencies are a function of maximum vibration velocity so that the larger the velocity, the more pronounced the discrepancy between the linear and nonlinear frequencies become. In Fig. 6, as the nondimensional maximum torsional vibration velocity increase, the nonlinear radial natural frequency increases while nonlinear torsional natural frequency becomes constant. It means that in coupled nonlinear vibration of CNTs, the nonlinear torsional natural frequency is independent to maximum torsional vibration velocity. In Fig. 7, as the nondimensional maximum radial vibration velocity increases, the nonlinear torsional natural frequency increases while there is a minimum point in the nonlinear radial natural frequency curve. It means that with increasing nondimensional maximum radial vibration velocity, the nonlinear radial natural frequency first decreases and then increases. This minimum can be obtained by differentiating nonlinear radial natural frequency with respect to nondimensional maximum radial vibration velocity. It should be noted that in the case $B = 0$ in Eq. (78) and also $D = E = 0$ in Eq. (79), the results are in an excellent agreement with those obtained via linear method according to the formulations presented in [41, 46].

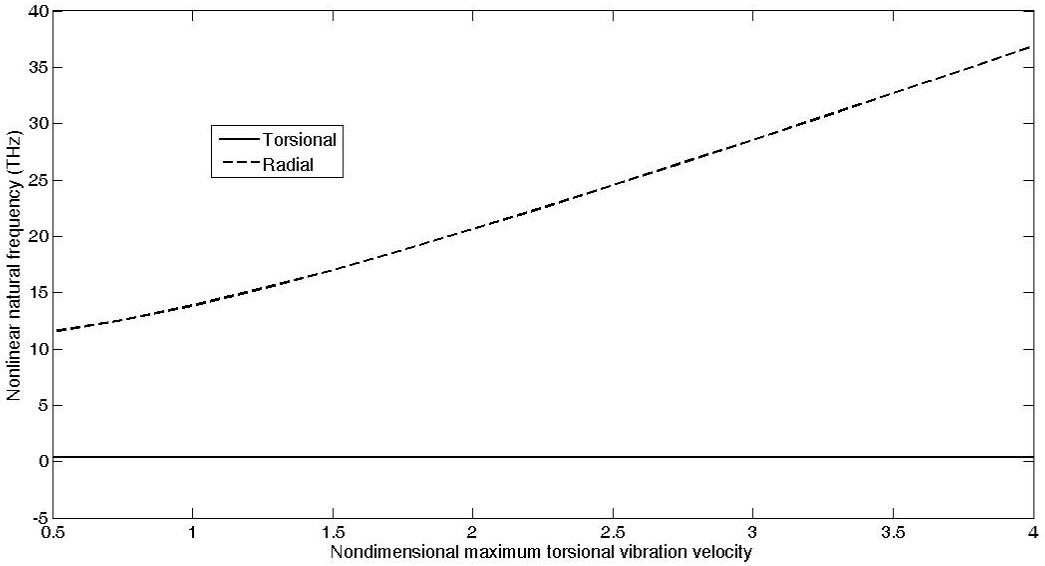

Fig. 6 Nonlinear natural frequencies against nondimensional maximum torsional vibration velocity for Zigzag (16, 0) SWCNTs with $Y=1$ under clamped-free boundary condition

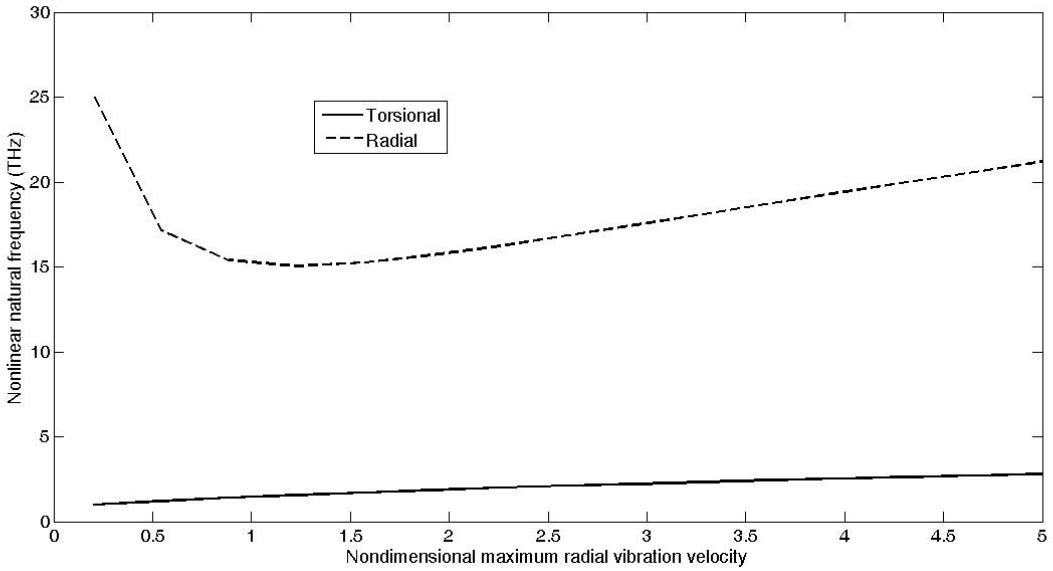

Fig. 7 Nonlinear natural frequencies against nondimensional maximum radial vibration velocity for Zigzag (16, 0) SWCNTs with $X=1$ under clamped-free boundary condition

Fig. 8 illustrates the nonlinear natural frequencies variation against to the tube length of Zigzag (16, 0) SWCNT under different boundary conditions. It can be observed that with the increase of the tube length, the nonlinear torsional natural frequencies of SWCNTs decrease while the radial one is constant. The decreasing rate for the nonlinear torsional natural frequency is more apparent for lower lengths. As is expected, the clamped CNT has the highest natural frequency among the selected boundary conditions. It is also seen that as the tube length increases, the nonlinear torsional natural frequencies tend to approach the linear ones especially for large

lengths. It can also be seen that in the same conditions, nonlinear radial natural frequency is much higher than the torsional one. This discrepancy is more apparent in lower lengths.

Variation of nonlinear natural frequencies versus tube diameter has been plotted in Figs. 9 and 10 for different vibration modes, respectively. As seen from these figures, as the tube diameter increases the nonlinear natural frequencies increase. This increasing is more apparent in higher modes of vibration and higher tube diameter. It is also seen that as the vibration mode increases, the nonlinear natural frequency increases too.

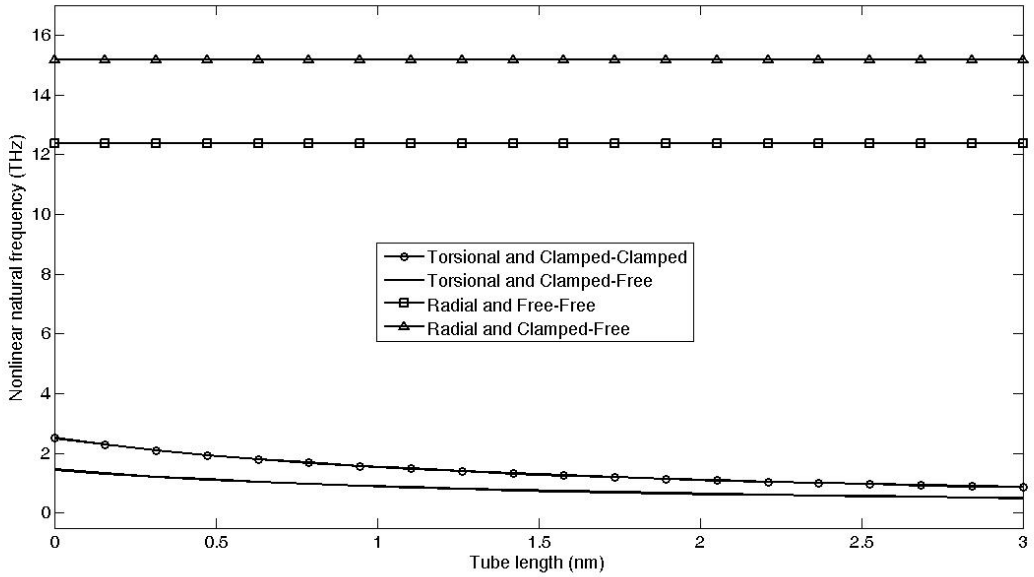

Fig. 8 Variation of nonlinear natural frequencies against tube length for Zigzag (16, 0) SWCNT with $X=1$ and $Y=1$ under various boundary conditions

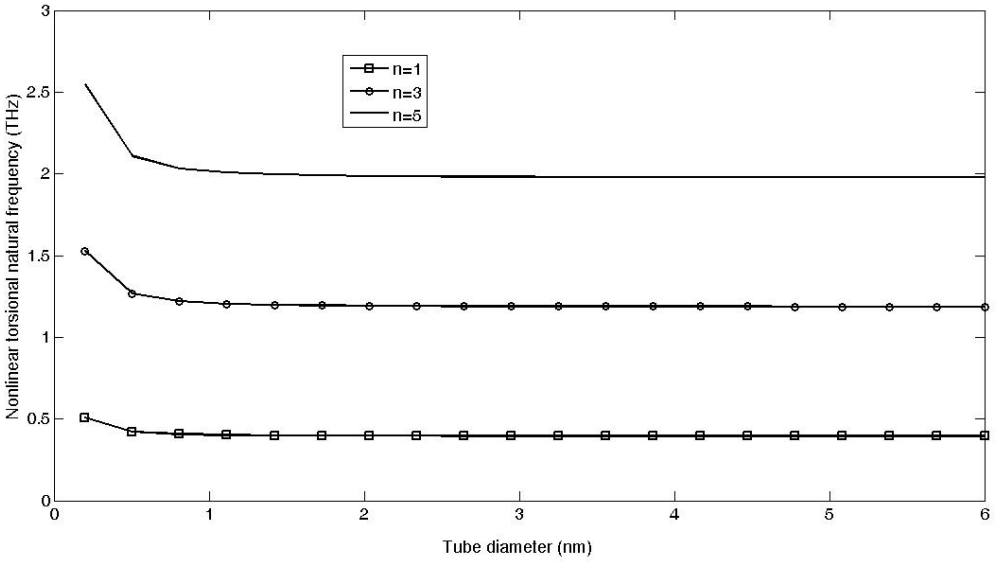

Fig. 9 Variation of nonlinear torsional natural frequencies versus tube diameter with $X=1$ and $Y=1$ for various modes of vibration

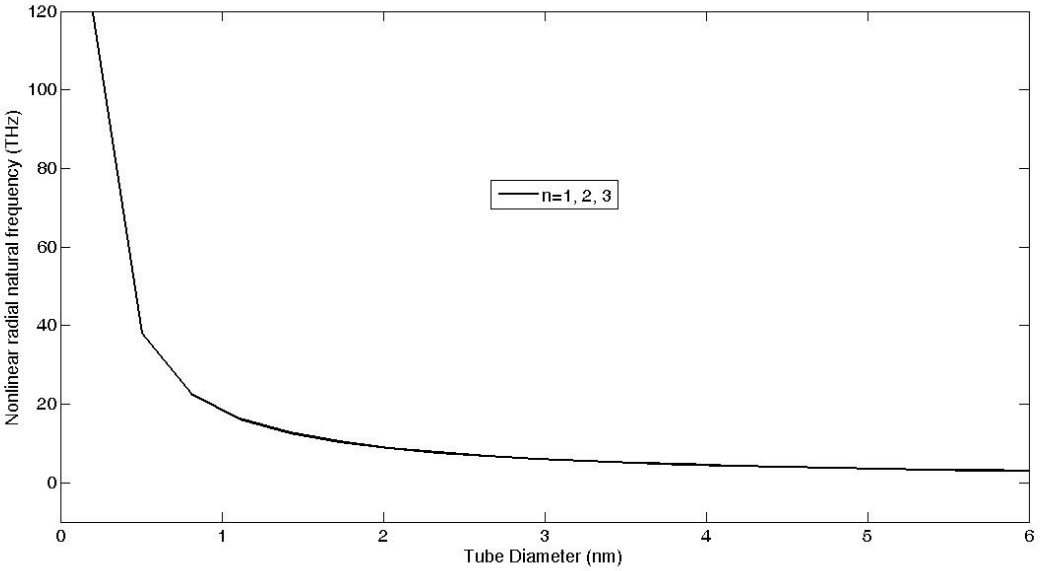

Fig. 10 Variation of nonlinear radial natural frequencies versus tube diameter with $X=1$ and $Y=1$ for various modes of vibration

1. Conclusions

In this paper, a detailed investigation of the nonlinear coupled torsional-radial vibration of SWCNTs based on HPM has been presented. The equations of motion for nonlinear coupled torsional-radial vibration of the SWCNT are derived based on nonlocal theory. It is the first time that nonlocal theory has been used to analyze the nonlinear coupled torsional-radial vibration of SWCNTs. The nonlinearities were originated from the large deformations in interaction of radial and torsional modes. To obtain the nonlinear frequency equations in coupled torsional-radial mode, the HPM has been used to derive the nonlinear natural frequencies of SWCNTs with arbitrary end conditions. The significant dependency of these nonlinear natural frequencies to tube radius, tube length and the maximum vibration velocity are studied in different boundary conditions and mode numbers. To show the accuracy and ability of this method, the generated results obtained have been compared with numerical results and excellent correlation has been achieved. The main results specifically obtained in this paper are as follows.

1- Due to the coupling of the torsional and radial vibrations and obtaining the nonlinear natural frequencies in radial and torsional modes of vibrations, radial and torsional nonlinear natural frequencies are defined in this analysis. The nondependent part of the nonlinear natural frequencies to the velocity of vibration represents the natural frequencies of the linear model in which the radial and torsional vibrations are decoupled.

2- The nonlinear natural frequencies of the system are obtained as the functions of maximum torsional and radial vibration velocities which this phenomenon is due to nonlinear nature of the system.

3- The coupling between the radial and torsional vibrations appears in the nonlinear higher order free vibrations of the SWCNT which is originated from the large deformation terms in the deriving of the nonlinear differential equations of the system. This interaction generally affects the global dynamic behavior of the SWCNT.

4- The nonlinearity leads to increment of the natural frequencies comparing with the linear model such that the nonlinear natural frequencies are higher than its linear counterparts.

5- As one travels through the free end conditions to clamped one, respectively, the influence of the boundary conditions is shown to increase the natural frequencies. This effect is more significant for lower tube lengths.

6- For same tube length/diameter, the absolute value of the nonlinear radial natural frequency is higher than of the nonlinear torsional natural frequency. This discrepancy is more apparent in higher mode numbers.

7- For equal maximum vibration velocities, the nonlinear radial natural frequency is higher than the torsional one. This difference between the radial and torsional nonlinear natural frequencies is more evident in higher vibration modes and lower tube length.

8- As the tube length increase, the natural frequencies decrease. This decreasing is more apparent in clamped boundary condition. This shows that the effect of interaction of the radial and torsional vibrations of the SWCNTs decreases with increase in tube length.

9- As the tube diameter increases, the natural frequencies decrease. For torsional natural frequency, this decreasing is more apparent in higher vibration mode while the radial natural frequency is insensitive to mode number. As the tube diameter increases more, the natural frequencies converge to single value. This shows that the effect of interaction of the radial and torsional vibrations of the SWCNTs decreases with increase in tube diameter.

References

[1] A. Fatahi□Vajari, "A new method for evaluating the natural frequency in radial breathing like mode vibration of double□walled carbon nanotubes," *ZAMM□Journal of Applied Mathematics and Mechanics/Zeitschrift für Angewandte Mathematik und Mechanik*, vol. 98, no. 2, pp. 255-269, 2018.

[2] M. Ferrari, V. Granik, and A. Imam, "Introduction to doublet mechanics," in *Advances in Doublet Mechanics*: Springer, 1997, pp. 1-26.

[3] M. Shishesaz, M. Shariati, and A. Yaghootian, "Nonlocal elasticity effect on linear vibration of nano-circular plate using adomian decomposition method," *Journal of Applied and Computational Mechanics*, vol. 6, no. 1, pp. 63-76, 2020.

[4] M. Pourabdy, M. Shishesaz, S. Shahrooi, and S. A. S. Roknizadeh, "Analysis of Axisymmetric Vibration of Functionally-Graded Circular Nano-Plate Based on the Integral Form of the Strain Gradient Model," *Journal of Applied and Computational Mechanics*, pp. -, 2021, doi: 10.22055/jacm.2021.37461.3021.

[5] A. Hadi, M. Z. Nejad, and M. Hosseini, "Vibrations of three-dimensionally graded nanobeams," *International Journal of Engineering Science*, vol. 128, pp. 12-23, 2018.

[6] A. Hadi, M. Z. Nejad, A. Rastgoo, and M. Hosseini, "Buckling analysis of FGM Euler-Bernoulli nano-beams with 3D-varying properties based on consistent couple-stress theory," *Steel and Composite Structures*, vol. 26, no. 6, pp. 663-672, 2018.

[7] M. Hosseini, H. H. Gorgani, M. Shishesaz, and A. Hadi, "Size-dependent stress analysis of single-wall carbon nanotube based on strain gradient theory," *International Journal of Applied Mechanics*, vol. 9, no. 06, p. 1750087, 2017.

[8] M. Hosseini, A. Hadi, A. Malekshahi, and M. Shishesaz, "A review of size-dependent elasticity for nanostructures," *Journal of Computational Applied Mechanics*, vol. 49, no. 1, pp. 197-211, 2018.

[9] M. Hosseini, M. Shishesaz, and A. Hadi, "Thermoelastic analysis of rotating functionally graded micro/nanodisks of variable thickness," *Thin-Walled Structures*, vol. 134, pp. 508-523, 2019.

[10] M. Hosseini, M. Shishesaz, K. N. Tahan, and A. Hadi, "Stress analysis of rotating nano-disks of variable thickness made of functionally graded materials," *International Journal of Engineering Science*, vol. 109, pp. 29-53, 2016.

[11] M. M. Khoram, M. Hosseini, A. Hadi, and M. Shishehsaz, "Bending Analysis of Bidirectional FGM Timoshenko Nanobeam Subjected to Mechanical and Magnetic Forces and Resting on Winkler–Pasternak Foundation," *International Journal of Applied Mechanics*, vol. 12, no. 08, p. 2050093, 2020.

[12] M. Mohammadi, M. Hosseini, M. Shishesaz, A. Hadi, and A. Rastgoo, "Primary and secondary resonance analysis of porous functionally graded nanobeam resting on a nonlinear foundation subjected to mechanical and electrical loads," *European Journal of Mechanics-A/Solids*, vol. 77, p. 103793, 2019.

[13] M. Mousavi Khoram, M. Hosseini, and M. Shishesaz, "A concise review of nano-plates," *Journal of Computational Applied Mechanics*, vol. 50, no. 2, pp. 420-429, 2019.

[14] M. Shishesaz and M. Hosseini, "Mechanical behavior of functionally graded nano-cylinders under radial pressure based on strain gradient theory," *Journal of Mechanics*, vol. 35, no. 4, pp. 441-454, 2019.

[15] M. Shishesaz, M. Hosseini, K. N. Tahan, and A. Hadi, "Analysis of functionally graded nanodisks under thermoelastic loading based on the strain gradient theory," *Acta Mechanica*, vol. 228, no. 12, pp. 4141-4168, 2017.

[16] S. M. Bachilo, M. S. Strano, C. Kittrell, R. H. Hauge, R. E. Smalley, and R. B. Weisman, "Structure-assigned optical spectra of single-walled carbon nanotubes," *science*, vol. 298, no. 5602, pp. 2361-2366, 2002.

[17] A. M. Rao *et al.*, "Diameter-selective Raman scattering from vibrational modes in carbon nanotubes," *Science*, vol. 275, no. 5297, pp. 187-191, 1997.

[18] S. Gupta and R. Batra, "Continuum structures equivalent in normal mode vibrations to single-walled carbon nanotubes," *Computational Materials Science*, vol. 43, no. 4, pp. 715-723, 2008.

[19] S. Gupta, F. Bosco, and R. Batra, "Wall thickness and elastic moduli of single-walled carbon nanotubes from frequencies of axial, torsional and inextensional modes of vibration," *Computational Materials Science*, vol. 47, no. 4, pp. 1049-1059, 2010.

[20] D. Sánchez-Portal, E. Artacho, J. M. Soler, A. Rubio, and P. Ordejón, "Ab initio structural, elastic, and vibrational properties of carbon nanotubes," *Physical Review B*, vol. 59, no. 19, pp. 12678-12688, 05/15/ 1999, doi: 10.1103/PhysRevB.59.12678.

[21] M. Shariati, B. Azizi, M. Hosseini, and M. Shishesaz, "On the calibration of size parameters related to non-classical continuum theories using molecular dynamics simulations," *International Journal of Engineering Science*, vol. 168, p. 103544, 2021.

[22] C. W. Lim, C. Li, and J. Yu, "Free torsional vibration of nanotubes based on nonlocal stress theory," *Journal of Sound and Vibration*, vol. 331, no. 12, pp. 2798-2808, 2012.

[23] M. M. Adeli, A. Hadi, M. Hosseini, and H. H. Gorgani, "Torsional vibration of nano-cone based on nonlocal strain gradient elasticity theory," *The European Physical Journal Plus*, vol. 132, no. 9, pp. 1-10, 2017.

[24] M. Shariati, M. Shishesaz, R. Mosalmani, S. A. Seyed Roknizadeh, and M. Hosseini, "Nonlocal effect on the axisymmetric nonlinear vibrational response of nano-disks using variational iteration method," *Journal of Computational Applied Mechanics*, vol. 52, no. 3, pp. 507-534, 2021.

[25] M. Shariati, M. Shishesaz, H. Sahbafar, M. Pourabdy, and M. Hosseini, "A review on stress-driven nonlocal elasticity theory," *Journal of Computational Applied Mechanics*, vol. 52, no. 3, pp. 535-552, 2021.

[26] M. Shishesaz, M. Shariati, and M. Hosseini, "Size effect analysis on Vibrational response of Functionally Graded annular nano plate based on Nonlocal stress-driven method," *International Journal of Structural Stability and Dynamics*, 2021, In press.

[27] M. Shariati, M. Shishesaz, R. Mosalmani, and S. A. S Roknizadeh, "Size Effect on the Axisymmetric Vibrational Response of Functionally Graded Circular Nano-Plate Based on the Nonlocal Stress-Driven Method," *Journal of Applied and Computational Mechanics*, 2021.

[28] M. Ebrahimian, A. Imam, and M. Najafi, "Doublet mechanical analysis of bending of Euler□Bernoulli and Timoshenko nanobeams," *ZAMM□Journal of Applied Mathematics and Mechanics/Zeitschrift für Angewandte Mathematik und Mechanik*, vol. 98, no. 9, pp. 1642-1665, 2018.

[29] M. Ebrahimian, A. Imam, and M. Najafi, "The effect of chirality on the torsion of nanotubes embedded in an elastic medium using doublet mechanics," *Indian Journal of Physics*, vol. 94, no. 1, pp. 31-45, 2020.

[30] A. Fatahi-Vajari and A. Imam, "Axial vibration of single-walled carbon nanotubes using doublet mechanics," *Indian Journal of Physics*, vol. 90, no. 4, pp. 447-455, 2016.

[31] A. Fatahi-Vajari and Z. Azimzadeh, "Analysis of nonlinear axial vibration of single-walled carbon nanotubes using Homotopy perturbation method," *Indian Journal of Physics*, vol. 92, no. 11, pp. 1425-1438, 2018.

[32] S. Iijima, "Helical microtubules of graphitic carbon," *nature*, vol. 354, no. 6348, pp. 56-58, 1991.

[33] A. Fatahi-Vajari and Z. Azimzadeh, "Axial vibration of single-walled carbon nanotubes with fractional damping using doublet mechanics," *Indian Journal of Physics*, vol. 94, no. 7, pp. 975-986, 2020.

[34] R. Ansari, R. Gholami, and H. Rouhi, "Vibration analysis of single-walled carbon nanotubes using different gradient elasticity theories," *Composites Part B: Engineering*, vol. 43, no. 8, pp. 2985-2989, 2012.

[35] I. Elishakoff and D. Pentaras, "Fundamental natural frequencies of double-walled carbon nanotubes," *Journal of Sound and Vibration*, vol. 322, no. 4-5, pp. 652-664, 2009.

[36] A. Fatahi-Vajari and A. Imam, "Lateral vibrations of single-layered graphene sheets using doublet mechanics," *Journal of Solid Mechanics*, vol. 8, no. 4, pp. 875-894, 2016.

[37] M. Arda and M. Aydogdu, "Analysis of free torsional vibration in carbon nanotubes embedded in a viscoelastic medium," *Advances in Science and Technology. Research Journal*, vol. 9, no. 26, 2015.

[38] A. Fatahi-Vajari and A. Imam, "Torsional vibration of single-walled carbon nanotubes using doublet mechanics," *Zeitschrift für angewandte Mathematik und Physik*, vol. 67, no. 4, pp. 1-22, 2016.

[39] M. Selim, "Torsional vibration of carbon nanotubes under initial compression stress," *Brazilian Journal of Physics*, vol. 40, pp. 283-287, 2010.

[40] Q. Li and M. Shi, "Intermittent transformation between radial breathing and flexural vibration modes in a single-walled carbon nanotube," *Proceedings of the Royal Society A: Mathematical, Physical and Engineering Sciences*, vol. 464, no. 2096, pp. 1941-1953, 2008.

[41] A. Fatahi□Vajari and A. Imam, "Analysis of radial breathing mode of vibration of single□walled carbon nanotubes via doublet mechanics," *ZAMM□Journal of Applied Mathematics and Mechanics/Zeitschrift für Angewandte Mathematik und Mechanik*, vol. 96, no. 9, pp. 1020-1032, 2016.

[42] M. Aydogdu, "Axial vibration analysis of nanorods (carbon nanotubes) embedded in an elastic medium using nonlocal elasticity," *Mechanics Research Communications*, vol. 43, pp. 34-40, 2012.

[43] S. Basirjafari, S. Esmaeilzadeh Khadem, and R. Malekfar, "Validation of shell theory for modeling the radial breathing mode of a single-walled carbon nanotube," *Int. J. Eng. Trans. A*, vol. 26, no. 4, pp. 447-454, 2013.

[44] J. Maultzsch, H. Telg, S. Reich, and C. Thomsen, "Radial breathing mode of single-walled carbon nanotubes: Optical transition energies and chiral-index assignment," *Physical Review B*, vol. 72, no. 20, p. 205438, 2005.

[45] S. Basirjafari, S. E. Khadem, and R. Malekfar, "Radial breathing mode frequencies of carbon nanotubes for determination of their diameters," *Current Applied Physics*, vol. 13, no. 3, pp. 599-609, 2013.

[46] J.-H. He, "Approximate analytical solution for seepage flow with fractional derivatives in porous media," *Computer Methods in Applied Mechanics and Engineering*, vol. 167, no. 1-2, pp. 57-68, 1998.

[47] J.-H. He, "Limit cycle and bifurcation of nonlinear problems," *Chaos, Solitons & Fractals*, vol. 26, no. 3, pp. 827-833, 2005.

[48] J.-H. He, "Homotopy perturbation technique," *Computer methods in applied mechanics and engineering*, vol. 178, no. 3-4, pp. 257-262, 1999.

[49] J.-H. He, "Some asymptotic methods for strongly nonlinear equations," *International journal of Modern physics B*, vol. 20, no. 10, pp. 1141-1199, 2006.

[50] M. Shishesaz, M. Shariati, A. Yaghootian, and A. Alizadeh, "Nonlinear Vibration Analysis of Nano-Disks Based on Nonlocal Elasticity Theory Using Homotopy Perturbation Method," *International Journal of Applied Mechanics*, vol. 11, no. 02, p. 1950011, 2019.

[51] A. Vahidi, Z. Azimzadeh, and M. Didgar, "An efficient method for solving Riccati equation using homotopy perturbation method," *Indian Journal of Physics*, vol. 87, no. 5, pp. 447-454, 2013.

[52] M. Ghasemia and K. M. TAVASSOLI, "Application of He's homotopy perturbation method to solve a diffusion-convection problem," 2010.

[53] Z. Azimzadeh, A. Vahidi, and E. Babolian, "Exact solutions for non-linear Duffing's equations by He's homotopy perturbation method," *Indian Journal of Physics*, vol. 86, no. 8, pp. 721-726, 2012.

[54] M. Ghasemi, M. T. Kajani, and A. Davari, "Numerical solution of two-dimensional nonlinear differential equation by homotopy perturbation method," *Applied Mathematics and Computation*, vol. 189, no. 1, pp. 341-345, 2007.

[55] A. P. Boresi, K. Chong, and J. D. Lee, *Elasticity in engineering mechanics*. John Wiley & Sons, 2010.